

# Scale-covariant and scale-invariant Gaussian derivative networks<sup>\*</sup>

Tony Lindeberg

Computational Brain Science Lab  
Division of Computational Science and Technology  
KTH Royal Institute of Technology, Stockholm, Sweden

**Abstract.** This paper presents a hybrid approach between scale-space theory and deep learning, where a deep learning architecture is constructed by coupling parameterized scale-space operations in cascade. By sharing the learnt parameters between multiple scale channels, and by using the transformation properties of the scale-space primitives under scaling transformations, the resulting network becomes provably scale covariant. By in addition performing max pooling over the multiple scale channels, a resulting network architecture for image classification also becomes provably scale invariant. We investigate the performance of such networks on the MNISTLargeScale dataset, which contains rescaled images from original MNIST over a factor 4 concerning training data and over a factor of 16 concerning testing data. It is demonstrated that the resulting approach allows for scale generalization, enabling good performance for classifying patterns at scales not present in the training data.

**Keywords:** scale covariance, scale invariance, scale generalisation, scale selection, Gaussian derivative, scale space, deep learning.

## 1 Introduction

A problem with traditional deep networks is that they are not covariant with respect scaling transformations in the image domain. In deep networks, non-linearities are performed relative to the current grid spacing, which implies that the deep network does not commute with scaling transformations.

One way of achieving scale covariance in a brute force manner is by applying the same deep net to multiply rescaled copies of the input image. Such an approach is developed and investigated in [1]. When working with such a scale-channel network it may, however, be harder to combine information from different scales, unless the multi-resolution representations at different levels of resolution are also resampled to a common reference frame when information from different scale levels is to be combined.

Another approach to achieve scale covariance is by applying multiple rescaled non-linear filters to the same image. For such an architecture, it will specifically

---

<sup>\*</sup> The support from the Swedish Research Council (contract 2018-03586) is gratefully acknowledged.

be easier to combine information from multiple scale levels, since the image data at all scales have the same resolution.

For the primitive discrete filters in a regular deep network, it is, however, not obvious how to rescale the primitive components, in terms of *e.g.*, local  $3 \times 3$  or  $5 \times 5$  filters or max pooling over  $2 \times 2$  neighbourhoods in a sufficiently accurate manner over continuous variations of spatial scaling factors. For this reason, it would be preferable to have a continuous model of the image filters, which are then combined together into suitable deep architectures, since the support regions of the continuous filters could then be rescaled in a continuous manner. Specifically, if we choose these filters as scale-space filters, which are designed to handle scaling transformations in image domain, we have the potential of constructing a rich family of hierarchical networks based on scale-space operations that are provably scale covariant [2].

The subject of this article is to develop and experimentally investigate one such hybrid approach between scale-space theory and deep learning. The idea that we shall follow is to define the layers in a deep architecture from scale-space operations, and then use the closed-form transformation properties of the scale-space primitives to achieve provable scale covariance and scale invariance of the resulting continuous deep network. Specifically, we will demonstrate that this will give the deep network the ability to generalize to previously unseen scales that are not present in the training data.

Technically, we will experimentally explore this idea for one specific type of architecture, where the layers are parameterized linear combinations of Gaussian derivatives up to order two. The overall principle for obtaining scale covariance and scale invariance is, however, much more general and applies to much wider classes of possible ways of defining layers from scale-space operations.

## 2 Relations to previous work

In classical computer vision, it has been demonstrated that scale-space theory constitutes a powerful paradigm for constructing scale-covariant and scale-invariant feature detectors and making visual operations robust to scaling transformations [3,4,5,6,7,8]. In the area of deep learning, a corresponding framework for handling general scaling transformations has so far not been as well established.

Concerning the relationship between deep networks and scale, several researchers have observed robustness problems of deep networks under scaling variations [9,10]. There have been some approaches developed to aim at scale invariant CNNs [11,12,13,14,15]. These approaches have, however, not been experimentally evaluated on the task of generalizing to scales not present in the training data [12,13,15], or only over a very narrow scale range [11,14].

Spatial transformer networks have been proposed as a general approach for handling image transformations in CNNs [16,17]. Plain transformation of feature maps by a spatial transformer is, however, not guaranteed to deliver a correct transformation, and may not support truly invariant recognition [18].

Concerning other deep learning approaches that somehow handle or are related to the notion of scale, deep networks have been applied to the multiple layers in an image pyramid [19,20,21,22], or using other multi-channel approaches where the input image is rescaled to different resolutions, possibly combined with interactions or pooling between the layers [23,24,25]. Variations or extensions of this approach include scale-dependent pooling [26], using sets of subnetworks in a multi-scale fashion [27], dilated convolutions [28,29,30], scale-adaptive convolutions [31] or adding additional branches of down-samplings and/or up-samplings in each layer of the network [32,33].

Scattering networks have been proposed based on Morlet wavelets [34,35,36]. Gabor functions have been proposed as primitives for modulating learned filters [37]. Affine Gaussian kernels have been used to compose free-form filters to adapt the receptive field size and shape to the image data [38].

Deep networks have been applied to spatially warped image data prior to image filter by a log-polar transformation [39,40], implying that the scaling transformation is mapped to a mere translation in the log-polar domain. Approaches to handling image transformations in deep networks have also been developed based on formalism from group theory [41,42,43,44].

Concerning the notion of scale covariance and its relation to scale generalization, a general sufficiency result was presented in [2] that guarantees provable scale covariance for hierarchical networks that are constructed from continuous layers defined from partial derivatives or differential invariants expressed in terms of scale-normalized derivatives. This idea was developed in more detail for a hand-crafted quasi quadrature network, with the layers representing idealized models of complex cells, and experimentally applied to the task of texture classification. It was demonstrated that the resulting approach allowed for scale generalization on the KTH-TIPS2 dataset, enabling classification of texture samples at scales not present in the training data.

The idea of modelling layers in neural networks as continuous functions instead of discrete filters has also been advocated in [45] and [46].

Concerning scale generalization for CNN:s, [1] presented a multi-scale-channel approach, where the same discrete CNN was applied to multiple scaled copies of each input image. It was demonstrated that the resulting scale-channel architectures were much more robust to scaling transformations than a regular vanilla CNN, and also that the resulting approach lead to good scale generalization, for classifying image patterns at scales not present in the training data.

The subject of this article is to complement these latter works, and specifically combine a specific instance of the general class of scale-covariant networks in [2] with deep learning, where we specifically will choose the continuous layers as linear combinations of Gaussian derivatives and demonstrate how such an architecture allows for scale generalization.

### 3 Gaussian derivative networks

In a traditional deep network, the filter weights are usually free variables with few additional constraints. In scale-space theory, on the other hand, theoretical results have been presented showing that Gaussian kernels and their corresponding Gaussian derivatives constitute a canonical class of image operations [47,48,49,50,51,52,53,54,55,56,57]. In classical computer vision based on hand-crafted image features, it has been demonstrated that a large number of visual tasks can be successfully addressed by computing image features and image descriptors based on Gaussian derivatives, or approximations thereof, as the first layer of image features [3,4,58,5,6,59,7,8]. One could therefore raise the question if such Gaussian derivatives could also be used as computational primitives for constructing deep networks.

Motivated by the fact that a large number of visual tasks have been successfully addressed by first- and second-order Gaussian derivatives, which are the primitive filters in the Gaussian 2-jet, let us initially explore the consequences of using linear combinations of first- and second-order Gaussian derivatives as the class of possible primitive filter weights in a deep network. Thus, given an image  $f$ , which could either be the input image to the deep net, or some higher layer  $F_k$  in the deep network, we first compute its scale-space representation by smoothing with the Gaussian kernel

$$L(x, y; \sigma) = (g(\cdot, \cdot; \sigma) * f(\cdot, \cdot))(x, y), \quad (1)$$

where

$$g(x, y; \sigma) = \frac{1}{2\pi\sigma^2} e^{-(x^2+y^2)/2\sigma^2}. \quad (2)$$

Then, for simplicity with the notation for the scale parameter  $\sigma$  suppressed, we consider arbitrary linear combinations of first- and second-order Gaussian derivatives as the class of possible linear filtering operations on  $f$  (or correspondingly for  $F_k$ ):

$$J_2(f) = C_x L_\xi + C_y L_\eta + \frac{1}{2}(C_{xx} L_{\xi\xi} + 2C_{xy} L_{\xi\eta} + C_{yy} L_{\eta\eta}), \quad (3)$$

where  $L_\xi$ ,  $L_\eta$ ,  $L_{\xi\xi}$ ,  $L_{\xi\eta}$  and  $L_{\eta\eta}$  are first- and second-order scale-normalized derivatives according to  $L_\xi = \sigma L_x$ ,  $L_\eta = \sigma L_y$ ,  $L_{\xi\xi} = \sigma^2 L_{xx}$ ,  $L_{\xi\eta} = \sigma^2 L_{xy}$  and  $L_{\eta\eta} = \sigma^2 L_{yy}$  (see Figure 1 for an illustration of the Gaussian derivative kernels).

Since directional derivatives can be computed as linear combinations of partial derivatives, for first- and second-order derivatives we have (see Figure 2 for an illustration)

$$L_\varphi = \cos \varphi L_x + \sin \varphi L_y, \quad (4)$$

$$L_{\varphi\varphi} = \cos^2 \varphi L_{xx} + 2 \cos \varphi \sin \varphi L_{xy} + \sin^2 \varphi L_{yy}, \quad (5)$$

it follows that the parameterized second-order kernels of the form (3) span all possible linear combinations of first- and second-order directional derivatives.

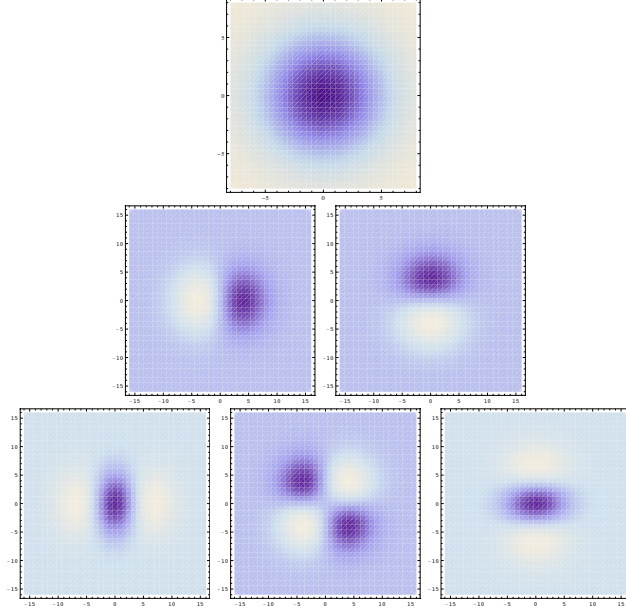


**Fig. 1.** The 2-D Gaussian kernel with its Cartesian partial derivatives up to order two for  $\sigma = 4$ .

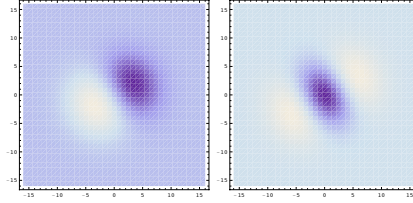


**Fig. 2.** First- and second-order directional derivatives of the 2-D Gaussian kernel computed from linear combinations of Cartesian partial derivatives according to equations (4) and (5) for  $\sigma = 4$  and  $\varphi = \pi/6$ .

The corresponding affine extension of such receptive fields, by replacing the rotationally symmetric Gaussian kernel (2) for scale-space smoothing by a corresponding affine Gaussian kernel, does also constitute a good idealized model for the receptive fields of simple cells in the primary visual cortex [57,60].

In contrast to previous work in computer vision or functional modelling of biological visual receptive fields, where such receptive fields are used as a first layer of linear receptive fields, we will, however, here investigate the consequences of coupling such receptive fields in cascade to form deep hierarchical image representations.

When coupling several of such smoothing stages in cascade, for example in combination with non-linear ReLU stages in between, it is natural to let the scale

parameter for layer  $k$  be proportional to an initial scale level  $\sigma_0$ , such that the scale parameter  $\sigma_k$  in layer  $k$  is  $\sigma_k = \beta_k \sigma_0$  for some set of  $\beta_k \geq \beta_{k-1} \geq 1$  and some minimum scale level  $\sigma_0 > 0$ . Specifically, it is natural to choose the relative scale parameter factors according to a geometric distribution

$$\sigma_k = r^{k-1} \sigma_0 \quad (6)$$

for some  $r \geq 1$ .

A similar idea of using Gaussian derivatives as structured receptive fields in convolutional networks has also been explored in [61], although not in the relation to scale covariance or using a self-similar sampling of the scale levels.

$$\begin{array}{ccc}
 F_k & \xrightarrow{F'_k(x',y';\sigma')=F_k(x,y;\sigma)} & F'_k \\
 \mathcal{J}_{2,\sigma_k} \uparrow & & \uparrow \mathcal{J}'_{k,\sigma'_k} \\
 \vdots & & \vdots \\
 \mathcal{J}_{2,\sigma_3} \uparrow & & \uparrow \mathcal{J}'_{2,\sigma'_3} \\
 F_2 & \xrightarrow{F'_2(x',y';\sigma')=F_2(x,y;\sigma)} & F'_2 \\
 \mathcal{J}_{2,\sigma_2} \uparrow & & \uparrow \mathcal{J}'_{2,\sigma'_2} \\
 F_1 & \xrightarrow{F'_1(x',y';\sigma')=F_1(x,y;\sigma)} & F'_1 \\
 \mathcal{J}_{2,\sigma_1} \uparrow & & \uparrow \mathcal{J}'_{2,\sigma'_1} \\
 f & \xrightarrow{x'=Sx,y'=Sy,\sigma'=S\sigma} & f'
 \end{array}$$

**Fig. 3.** Commutative diagram for a scale-covariant Gaussian derivative network constructed by coupling linear combinations of scale-normalized Gaussian derivatives in cascade, with non-linear ReLu stages in between. Because of the transformation properties of the individual layers under scaling transformations, it will be possible to perfectly match the corresponding layers  $F_k$  and  $F'_k$  under a scaling transformation of the underlying image domain  $f'(x') = f(x)$  for  $x' = Sx$  and  $y' = Sy$ , provided that the scale parameter  $\sigma_k$  in layer  $k$  is proportional to the scale parameter  $\sigma_1$  in the first layer,  $\sigma_k = r_k^2 \sigma_1$ , for some scalar constant  $r_k$ . For such a network, the scale parameters in the two domains should be related according to  $\sigma'_k = S\sigma_k$ .

### 3.1 Provable scale covariance

To prove that a deep network constructed by coupling linear filtering operations of the form (3) with pointwise non-linearities in between becomes scale covariant, let us consider two images  $f$  and  $f'$  that are related by a scaling transformation  $f'(x', y') = f(x, y)$  for  $x' = Sx$ ,  $y' = Sy$  and some spatial scaling factor  $S > 0$ .

If the scale parameters  $\sigma$  and  $\sigma'$  in the two domains are related according to  $\sigma' = S\sigma$ , then it follows from a general result in [3, Eq. (20)] that the scale-normalized derivatives will be equal (when using scale normalization power  $\gamma = 1$  in the scale-normalized derivative concept):

$$L'_{\xi\alpha\eta\beta}(x', y'; \sigma') = L_{\xi\alpha\eta\beta}(x, y; \sigma). \quad (7)$$

Thus, given that the image positions and the scale levels are appropriately matched according to  $x' = Sx$ ,  $y' = Sy$  and  $\sigma' = S\sigma$ , it holds that the first layers  $F_1$  and  $F'_1$  will be equal up to a scaling transformation:

$$F'_1(x', y'; \sigma') = J'_2(f')(x', y'; \sigma') = J_2(f)(x, y; \sigma) = F_1(x, y; \sigma). \quad (8)$$

By continuing a corresponding construction of higher layers, by applying similar operations in cascade, with the initial scale levels  $\sigma_0$  and  $\sigma'_0$  in (6) related according to  $\sigma'_0 = S\sigma_0$ , it follows that also the higher layers in the hierarchy will be equal up to a scaling transformation (see Figure 3 for an illustration):

$$F'_k(x', y'; \sigma') = F_k(x, y; \sigma). \quad (9)$$

A pointwise non-linearity, such as a ReLu stage, trivially commutes with scaling transformations and does therefore not affect the scale covariance properties.

### 3.2 Provable scale invariance

To prove scale invariance after max pooling, let us assume that we have an *infinite* set of scale channels  $\mathcal{S}$ , either continuously distributed with  $\mathcal{S} = \{\sigma \in \mathbb{R}_+\}$  or discrete with  $\mathcal{S} = \{\sigma_i = \gamma^i, \forall i \in \mathbb{Z} \text{ for some } \gamma > 1\}$ . The max pooling operation will then at every image position  $(x, y)$  return the value

$$F_{k,sup}(x, y) = \sup_{\sigma \in \mathcal{S}} F_k(x, y; \sigma) \quad (10)$$

Let us without essential loss of generality assume that the scaling transformation is performed around the image point  $(x, y)$ , implying that we can without essential loss of generality assume that the origin is located at this point. The set of feature values before the scaling transformation is therefore given by

$$M = \{F_k(0, 0; \sigma) \forall \sigma\} \quad (11)$$

and the set of feature values after the scaling transformation

$$M' = \{F'_k(0, 0; \sigma') \forall \sigma'\}. \quad (12)$$

With the relationship  $\sigma' = S\sigma$ , these sets are clearly equal provided that  $S > 0$  in the continuous case or  $S = \gamma^j$  for some  $j \in \mathbb{Z}$  in the discrete case, implying that the supremum of the set is preserved (or the result of any other permutation invariant pooling operation, such as the average).

In this way, the result after max pooling is essentially scale invariant, in the sense that the result of the max pooling operation at any image point follows the geometric transformation of the image point under scaling transformations.

When using a *finite* number of scale channels, the result of max pooling is, however, not guaranteed to truly scale invariant, since there could be boundary effects, implying that the maximum over scales moves in or out from a finite scale interval because of the scaling transformation that shifts the position of the scale maxima on the scale axis. To reduce the likelihood of such effects occurring, we propose as design criterion to ensure that there should be a sufficient number of additional scale channels below and above the effective training scales, so that the learning algorithm could learn that the image structures that occur below and above the effective training scales are less relevant, and thereby associate lower values of the feature maps to such image structures, and thereby reducing the likelihood that erroneous types of image structures are picked up by the max pooling operation over the multiple scale channels.

A similar scale boundary handling strategy is used in the scale channel networks based on applying a fixed CNN to a set of rescalings of the original image in [1], as opposed to the approach here based on applying a set of rescaled CNNs to a fixed size input image.

## 4 Experiments with a single-scale-channel network

To investigate the ability of these types of deep hierarchical Gaussian derivative networks to capture image structures with different image shapes, we first did initial experiments with the regular MNIST dataset [62]. We constructed a 6-layer network in PyTorch with 12-14-16-20-64 channels in the intermediate layers and 10 output channels, with a final layer of max-pooling applied to the 10 output channels, intended to learn each type of digit. We chose the initial scale level  $\sigma_0 = 0.9$  pixels and the relative scale ratio  $r = 1.25$  in (6), implying that the maximum value of  $\sigma$  is  $0.9 \times 1.25^5 \approx 2.7$  pixels relative to the image size of  $28 \times 28$  pixels. The individual receptive fields do then have larger spatial extent because of the spatial extent of the Gaussian kernels used for image smoothing and the larger positive and negative side lobes of the first- and second-order derivatives.

We used regular ReLu stages between the filtering steps, but no spatial max pooling or spatial stride, and no fully connected layer, since such operations would destroy the scale covariance. Instead, the receptive fields are solely determined from linear combinations of Gaussian derivatives, with successively larger receptive fields of size  $\sigma_0 r^{k-1}$ , which enable a gradual integration from local to regional image structures. In the final layer, only the value at the central pixel is extracted, or here for an even image size, the average over the central  $2 \times 2$  neighbourhood, which, however, destroys full scale covariance. To ensure full scale covariance, the input images should instead have odd image size.

The network was trained on 50 000 images in the dataset, with a bias term  $C_0$  and the parameters  $C_x$ ,  $C_y$ ,  $C_{xx}$ ,  $C_{xy}$  and  $C_{yy}$  in (3) initiated to random values and trained individually for each layer and feature channel by stochastic gradient



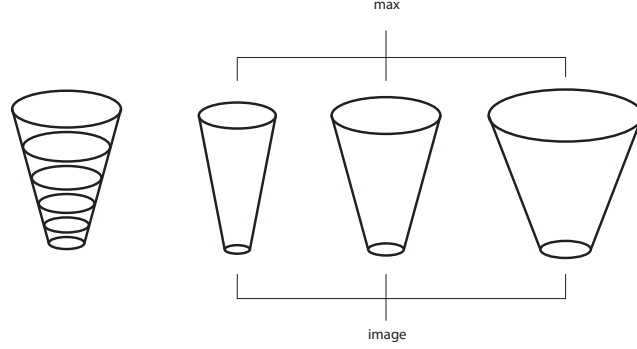


**Fig. 4.** (left) Schematic illustration of the architecture of the single-scale-channel network, with 6 layers of receptive fields at successively coarser levels of scale. (right) Schematic illustration of the architecture of a multi-scale-channel network, with multiple parallel scale channels over a self-similar distribution of the lowest scale level.

descent over 40 epochs using the Adam optimizer [63] set to minimize the binary cross-entropy loss using a cosine learning curve with maximum learning rate of 0.01 and minimum learning rate 0.00005 and using batch normalization over batches with 50 images. The experiment lead to 99.93 % training accuracy and 99.43 % test accuracy on the test dataset containing 10 000 images.

Notably, the training accuracy does not reach 100.00 %, probably because of the restricted shapes of the filter weights, as determined by the *a priori* shapes of the receptive fields in terms of linear combinations of first- and second-order Gaussian derivatives. Nevertheless, the test accuracy is quite good given the moderate number of parameters in the network ( $6 \times (12 + 12 \times 14 + 14 \times 16 + 16 \times 20 + 20 \times 64 + 64 \times 10) = 15\,864$ ).

#### 4.1 Discrete implementation

In the numerical implementation of scale-space smoothing, we used separable smoothing with the discrete analogue of the Gaussian kernel  $T(n; s) = e^{-s} I_n(s)$  for  $s = \sigma^2$  in terms of modified Bessel functions  $I_n$  of integer order [64]. The discrete derivative approximations were computed by central differences,  $\delta_x = (-1/2, 0, 1/2)$ ,  $\delta_{xx} = (1, -2, 1)$ ,  $\delta_{xy} = \delta_x \delta_y$ , etc., implying that the spatial smoothing operation can be shared between derivatives of different order, and implying that scale-space properties are preserved in the discrete implementation of the Gaussian derivatives [65]. This is a general methodology for computing Gaussian derivatives for a large number of visual tasks.

By computing the Gaussian derivative responses in this way, the scale-space smoothing is only performed once for each scale level, and there is no need for repeating the scale-space smoothing for each order of the Gaussian derivatives.

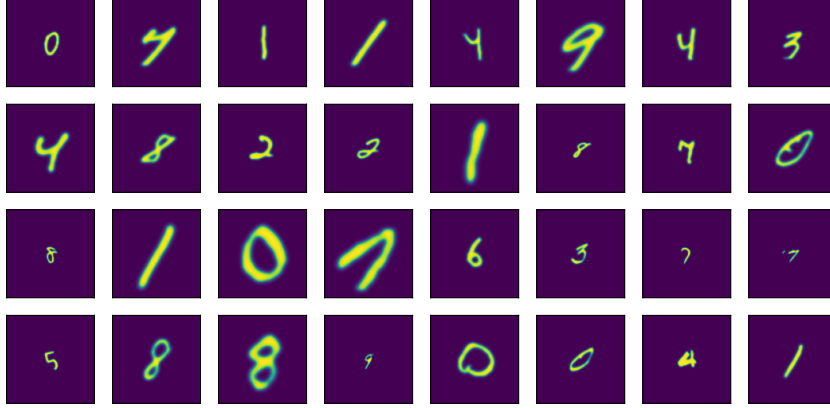


**Fig. 5.** Sample images from the MNISTLargeScale dataset [1,66]. This figure shows digits for sizes in the range  $[1, 4]$ , for which there are training data. In addition, the MNISTLargeScale dataset contains testing data over the wider size range  $[1/2, 8]$ .

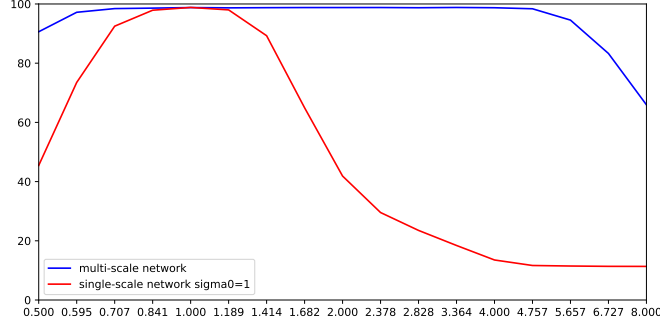
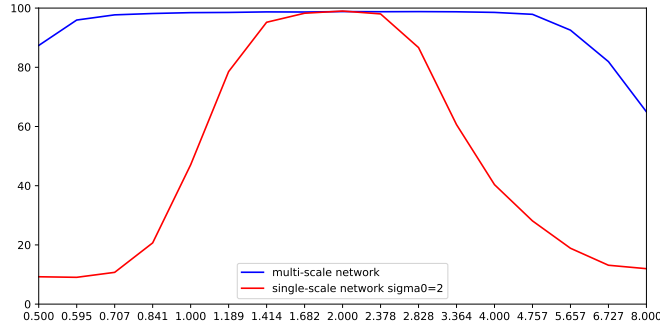
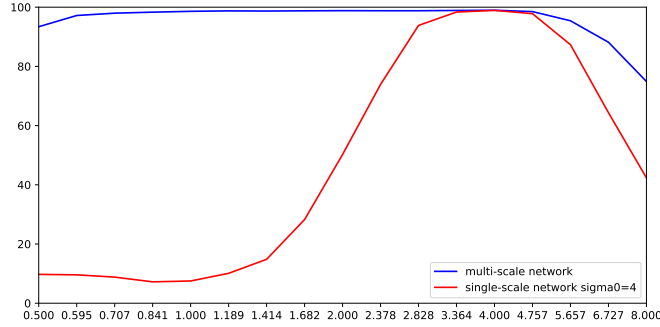
## 5 Experiments with a multi-scale-channel network

To investigate the ability of a multi-scale-channel network to handle spatial scaling transformations, we made experiments on the MNISTLargeScale dataset [1,66]. This dataset contains rescaled digits from the original MNIST dataset [62] embedded in images of size  $112 \times 112$ , see Figure 5 for an illustration. For training, the dataset contains 50 000 rescaled digits with relative scale factors 1, 2 and 4, respectively, henceforth referred to as sizes 1, 2 and 4. For testing, the dataset contains 10 000 rescaled digits with relative scale factors between  $1/2$  and 8, respectively, with a relative scale ratio of  $\sqrt[4]{2}$  between adjacent sizes.

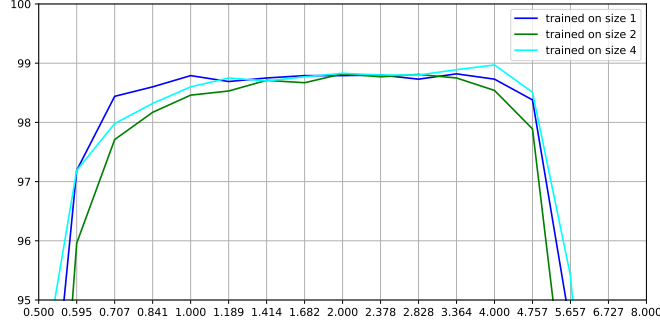
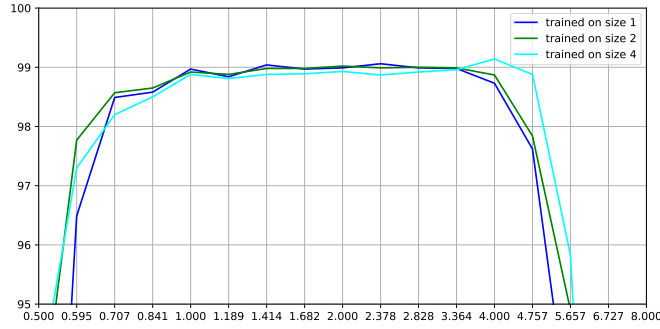
For making experiments with a multi-scale-channel architecture, we created a multi-scale-channel network with 8 scale channels with their lowest scale values  $\sigma_0$  between  $1/\sqrt{2}$  and 8 and a scale ratio of  $\sqrt{2}$  between adjacent scale channels. For each channel, we used a Gaussian derivative network of similar architecture as the single-scale-channel network, with 12-14-16-20-64 channels in the intermediate layers and 10 output channels, and with a relative scale ratio  $r = 1.25$  (6) between adjacent layers, implying that the maximum value of  $\sigma$  in each channel is  $\sigma_0 \times 1.25^5 \approx 3.1 \sigma_0$  pixels.

Importantly, the parameters  $C_0$  and  $C_x, C_y, C_{xx}, C_{xy}$  and  $C_{yy}$  in (3) are shared between the scale channels, implying that the scale channels themselves are truly scale covariant, because of the parameterization of the receptive fields in terms of scale-normalized Gaussian derivatives. The batch normalization stage is also shared between the scale channels. The output from max pooling over the scale channels is furthermore truly scale invariant, if we assume an infinite number of scale channels so that scale boundary effects can be disregarded.

Figure 6 shows the result of an experiment to investigate the ability of such a multi-scale-channel network to generalize to testing at scales not present in the training data.

*Scale generalization performance when training on size 1**Scale generalization performance when training on size 2**Scale generalization performance when training on size 4*

**Fig. 6.** Experiments showing the ability of a multi-scale-channel network to generalize to new scale levels not present in the training data. In the top row, all training data are for size 1, whereas the testing data are for all sizes between  $1/2$  and 8. The red curve shows the generalization performance for a single-scale-channel network for  $\sigma_0 = 1$ , whereas the blue curve shows the result for a multi-scale-channel network covering the range of  $\sigma_0$ -values between  $1/\sqrt{2}$  and 8. As can be seen from the result, the generalization ability is much better for the multi-scale-channel network compared to the single-scale-channel network. In the middle row, a similar type of experiment is repeated for training size 2 and with  $\sigma_0 = 2$  for the single-scale-channel network. In the bottom row, a similar experiment is performed for training size 4 and with  $\sigma_0 = 4$  for the single-scale-channel network. (Horizontal axis: Scale of testing data.)

*Scale generalization performance when training on different sizes: Default network**Scale generalization performance when training on different sizes: Larger network*

**Fig. 7.** Joint visualization of the generalization performance when training a multi-scale-channel Gaussian derivative network on training data with sizes 1, 2 and 4, respectively. As can be seen from the graphs, the performance is rather similar for all these networks over the size range between 1 and 4, a range for which the discretization errors in the discrete implementation can be expected to be low (a problem too fine scales) and the influence of boundary effects causing a mismatch between what parts of the digits are visible in the testing data compared to a training data (a problem at too coarse scales). The top figure shows the results for the default network with 12-16-24-32-64-10 feature channels. The bottom figure shows the results for a larger network with 16-24-32-48-64-10 feature channels. (Horizontal axis: Scale of testing data.)

For the experiment shown in the top figure, we have used 50 000 training images of size 1, and 10 000 testing images for each one of the 19 sizes between  $1/2$  and 8 with a relative size ratio of  $\sqrt[4]{2}$  between adjacent sizes. The red curve shows the generalization performance for a single-scale-channel network with  $\sigma_0 = 1$ , whereas the blue curve shows the generalization performance for the multi-scale-channel network with 8 scale channels between  $1/\sqrt{2}$  and 8.

As can be seen from the graphs, the generalization performance is quite good for the multi-scale-channel network, for sizes in roughly in the range  $1/\sqrt{2}$  and

$4\sqrt{2}$ . For smaller sizes near  $1/2$ , there are discretization problems due to sampling artefacts and too fine scale levels relative to the grid spacing in the image, implying that the transformation properties under scaling transformations of the underlying Gaussian derivatives are not well approximated in the discrete implementation. For larger sizes near 8, there are problems due to boundary effects and that the entire digit is not visible in the testing stage, implying a mismatch between the training data and the testing data. Otherwise, the generalization performance is very good over the size range between 1 and 4.

For the single-scale-channel network, the generalization performance to scales far from the scales in the training data is on the other hand very poor.

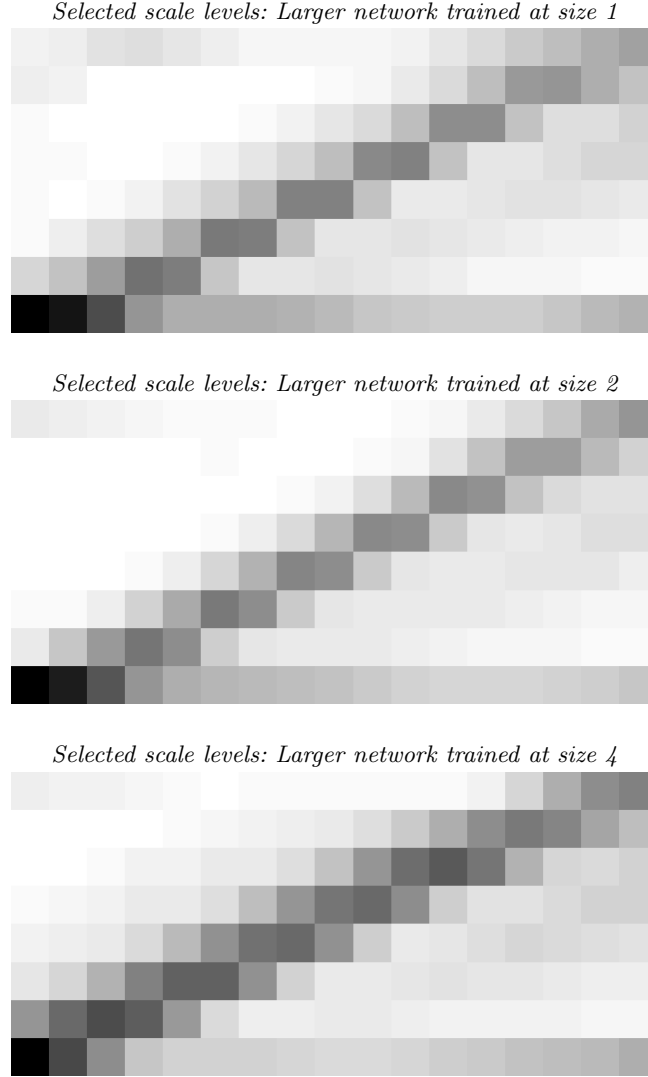
In the middle figure, we show the result of a similar experiment for training images of size 2 and with the lowest scale level  $\sigma_0 = 2$  for the single-scale-channel network. The bottom figure shows the result of a similar experiment performed with training images of size 4 and with the lowest scale level  $\sigma_0 = 4$  for the single-scale-channel network.

Figure 7 shows a joint visualization of the generalization performance for all these experiments, where we have also zoomed in on the top performance values in the range 98-99 %. In addition to the results from the default network with 12-16-24-32-64-10 feature channels, we do also show results obtained from a larger network with 16-24-32-48-64-10 feature channels, which has more degrees of freedom in the training stage and leads to better results. As can be seen from the graphs, the performance values for training sizes 1, 2 and 4, respectively, are quite similar for testing data with sizes in the range between 1 and 4, a size range for which the discretization errors in the discrete implementation can be expected to be low (a problem too fine scales) and the influence of boundary effects causing a mismatch between what parts of the digits are visible in the testing data compared to a training data (a problem at too coarse scales)

In this way, the experiment demonstrates that it is possible to use the combination of (i) scale-space features as computational primitives for a deep learning method with (ii) the closed-form transformation properties of the scale-space primitives under scaling transformations to (iii) make a deep network generalize to new scale levels not spanned by the training data.

## 5.1 Scale selection properties

Since the Gaussian derivative network is expressed in terms of scale-normalized derivatives over multiple scales, and the max-pooling operation over the scale channels implies detecting maxima over scale, the resulting approach shares similarities to classical methods for scale selection based on local extrema over scales of scale-normalized derivatives [3,4,67]. The approach is also closely related to the scale selection approach in [68,69] based on choosing the scales at which a supervised classifier delivers class labels with the highest posterior. A limitation of choosing only a single maximum over scales compared to processing multiple local extrema over scales as in [3], however, is that the approach may be sensitive to boundary effects at the scale boundaries, implying that the scale generaliza-



**Fig. 8.** Visualization of the scale channels that are selected in the max pooling stage, when training the larger network for each one of the sizes 1, 2 and 4. For each testing size, shown on the horizontal axis, the vertical axis displays a histogram of the scale levels at which the maximum over the scale channels is assumed for the different samples in the testing set, with the lowest scale at the bottom and the highest scale at the top. As can be seen from the figure, there is a general tendency of the composed classification scheme to select coarser scale levels with increasing size of the image structures, in agreement with the conceptual similarity to classical methods for scale selection based on detecting local extrema over scales of scale-normalized derivatives, the difference being that here only the global maximum over scale is used. (Note that the grey-level values are not directly comparable between the three images, since the grey-levels have been rescaled according to the maximum value in each case, which differs between the three experiments, and is, in particular, somewhat different for training size 4 compared to training sizes 1 and 2.)

tion properties may be affected depending on how many coarser-scale and/or finer-scale channels are being processed relative to the scale of the image data.

In Figure 8, we have visualized the scale selection properties when applying these multi-scale-channel Gaussian derivative network to the MNISTLargeScale dataset. For each one of the training sizes 1, 2 and 4, we show what scales are selected as function of the testing scale. Specifically, for each testing scale, shown on the horizontal axis, we display a histogram of the scale channels at which the maximum over scales is assumed over all the samples in the testing set, with the smallest scale at the bottom and the largest scale at the top.

As can be seen from the figure, the network has an overall tendency of selecting coarser scale levels with increasing size of the image structures it is applied to. Specifically, the overall tendency is that the selected scale is proportional to the size of the testing data, in agreement with the theory for scale selection based on local extrema over scales of scale-normalized derivatives.

## 5.2 Properties of the multi-scale-channel network training

Notably, the scale selection signatures in Figure 8 are roughly similar for training performed at the different training sizes 1, 2, and 4, demonstrating an overall agreement between the theoretical predictions from the scale-invariant properties of the Gaussian derivative networks and the experiments. The scale selection signatures are, however, not fully identical, which can be explained from the fact that the training error is far from zero, implying that the net effects of the training error on the properties of the network may be somewhat different when training the network on different datasets, here for different training sizes.

The results from training at sizes 1 *vs.* 2 are very similar, whereas there is a certain difference compared to training at size 4. A similar relationship can be seen in the scale generalization graphs in Figure 7.

There is also a slight tendency of these networks to choose the finest scale level for some samples in violation of the overall linear dependency of the selected scale channel as function of the size in the training data. A possible explanation for this is that the training procedure is agnostic to the selection of at what scale the maximum over scale should be chosen for a particular image sample, and may therefore choose to allocate the maximum over scale to different channels for different image samples, although the digits in those image samples have roughly similar size.

The training process is initiated randomly, and during the gradient descent optimization, the network has to learn to associate large values of the feature map for the appropriate class for each training sample in some scale channel, while also having to learn to not associate large values for erroneous classes for any other training samples in any other scale channel.

Training of a multi-scale-channel network could therefore be considered as a harder training problem than the training of a single channel network. Experimentally, we have also observed that the training error is significantly larger for a multi-scale-channel network than for a single-scale-channel network, and that

the training procedure had not converged fully after the 20 epochs that we used for training the multi-scale-channel networks.

A possible extension of this work, is therefore to perform a deeper study regarding the task of training multi-scale-channel networks, and investigate if this training task calls for other training strategies than used here, specifically considering that the computational primitives in the layers of the Gaussian derivative networks are also different from the computational primitives in regular CNNs.

Notwithstanding these possibilities for improvements in the training scheme, the experiments in the paper demonstrate that it is possible to use scale-space operations as computational primitives in deep networks, and to use the transformation properties of such computational primitives under scaling transformations to perform scale generalization, which is the main objective of this study.

## 6 Summary and discussion

We have presented a hybrid approach between scale-space theory and deep learning, where the layers in a hierarchical network architecture are modelled as continuous functions instead of discrete filters, and are specifically chosen as scale-space operations, here in terms of linear combinations of scale-normalized Gaussian derivatives. Experimentally, we have demonstrated that the resulting approach allows for scale generalization, to enable good performance for classifying image patterns at scales not spanned by the training data.

The work is intended as a proof-of-concept of the idea of using scale-space features as computational primitives in a deep learning method, and of using their closed-form transformation properties under scaling transformations to perform extrapolation or generalization to new scales not present in the training data.

Concerning the choice of Gaussian derivatives as computational primitives in the method, it should, however, be emphasized that the necessity results of scale-space theory only state that the first layer of receptive fields should be constructed in terms of Gaussian derivatives. Concerning higher layers, further studies should be performed concerning the possibilities of using other scale-space features in the higher layers, that may represent the variability of natural image structures more efficiently, within the generality of the sufficiency result for scale-covariant continuous hierarchical networks in [2].

## Acknowledgements

I would like to thank Ylva Jansson for sharing her code for training and testing networks in PyTorch.

## References

1. Jansson, Y., Lindeberg, T.: Exploring the ability of CNNs to generalise to previously unseen scales over wide scale ranges. In: International Conference on Pattern Recognition (ICPR 2020). (2021) Extended version in arXiv:2004.01536.



2. Lindeberg, T.: Provably scale-covariant continuous hierarchical networks based on scale-normalized differential expressions coupled in cascade. *Journal of Mathematical Imaging and Vision* **62** (2020) 120–148
3. Lindeberg, T.: Feature detection with automatic scale selection. *International Journal of Computer Vision* **30** (1998) 77–116
4. Lindeberg, T.: Edge detection and ridge detection with automatic scale selection. *International Journal of Computer Vision* **30** (1998) 117–154
5. Mikolajczyk, K., Schmid, C.: Scale and affine invariant interest point detectors. *International Journal of Computer Vision* **60** (2004) 63–86
6. Lowe, D.G.: Distinctive image features from scale-invariant keypoints. *International Journal of Computer Vision* **60** (2004) 91–110
7. Bay, H., Ess, A., Tuytelaars, T., van Gool, L.: Speeded up robust features (SURF). *Computer Vision and Image Understanding* **110** (2008) 346–359
8. Lindeberg, T.: Image matching using generalized scale-space interest points. *Journal of Mathematical Imaging and Vision* **52** (2015) 3–36
9. Fawzi, A., Frossard, P.: Manitest: Are classifiers really invariant? In: *British Machine Vision Conference (BMVC 2015)*. (2015)
10. Singh, B., Davis, L.S.: An analysis of scale invariance in object detection — SNIP. In: *Proc. Computer Vision and Pattern Recognition (CVPR 2018)*. (2018) 3578–3587
11. Xu, Y., Xiao, T., Zhang, J., Yang, K., Zhang, Z.: Scale-invariant convolutional neural networks. *arXiv preprint arXiv:1411.6369* (2014)
12. Kanazawa, A., Sharma, A., Jacobs, D.W.: Locally scale-invariant convolutional neural networks. *arXiv preprint arXiv:1412.5104* (2014)
13. Marcos, D., Kellenberger, B., Lobry, S., Tuia, D.: Scale equivariance in CNNs with vector fields. *arXiv preprint arXiv:1807.11783* (2018)
14. Ghosh, R., Gupta, A.K.: Scale steerable filters for locally scale-invariant convolutional neural networks. *arXiv preprint arXiv:1906.03861* (2019)
15. Worrall, D., Welling, M.: Deep scale-spaces: Equivariance over scale. In: *Advances in Neural Information Processing Systems*. (2019) 7366–7378
16. Jaderberg, M., Simonyan, K., Zisserman, A., Kavukcuoglu, K.: Spatial transformer networks. In: *Advances in Neural Information Processing Systems*. (2015) 2017–2025
17. Lin, C.H., Lucey, S.: Inverse compositional spatial transformer networks. In: *Proc. Computer Vision and Pattern Recognition (CVPR 2017)*. (2017) 2568–2576
18. Finnveden, L., Jansson, Y., Lindeberg, T.: Understanding when spatial transformer networks do not support invariance, and what to do about it. In: *International Conference on Pattern Recognition (ICPR 2020)*. (2021) Extended version in *arXiv:2004.11678*.
19. Lin, T.Y., Dollár, P., Girshick, R., He, K., Hariharan, B., Belongie, S.: Feature pyramid networks for object detection. In: *Proc. Computer Vision and Pattern Recognition (CVPR 2017)*. (2017)
20. Lin, T.Y., Goyal, P., Girshick, R., He, K., Dollár, P.: Focal loss for dense object detection. In: *Proc. International Conference on Computer Vision (ICCV 2017)*. (2017) 2980–2988
21. He, K., Gkioxari, G., Dollár, P., Girshick, R.: Mask R-CNN. In: *Proc. International Conference on Computer Vision (ICCV 2017)*. (2017) 2961–2969
22. Hu, P., Ramanan, D.: Finding tiny faces. In: *Proc. Computer Vision and Pattern Recognition (CVPR 2017)*. (2017) 951–959

23. Ren, S., He, K., Girshick, R., Zhang, X., Sun, J.: Object detection networks on convolutional feature maps. *IEEE Trans. Pattern Analysis and Machine Intell.* **39** (2016) 1476–1481
24. Nah, S., Kim, T.H., Lee, K.M.: Deep multi-scale convolutional neural network for dynamic scene deblurring. In: *Proc. Computer Vision and Pattern Recognition (CVPR 2017)*. (2017) 3883–3891
25. Chen, L.C., Papandreou, G., Kokkinos, I., Murphy, K., Yuille, A.L.: Deeplab: Semantic image segmentation with deep convolutional nets, atrous convolution, and fully connected CRFs. *IEEE Trans. Pattern Analysis and Machine Intell.* **40** (2017) 834–848
26. Yang, F., Choi, W., Lin, Y.: Exploit all the layers: Fast and accurate CNN object detector with scale dependent pooling and cascaded rejection classifiers. In: *Proc. Computer Vision and Pattern Recognition (CVPR 2016)*. (2016) 2129–2137
27. Cai, Z., Fan, Q., Feris, R.S., Vasconcelos, N.: A unified multi-scale deep convolutional neural network for fast object detection. In: *Proc. European Conference on Computer Vision (ECCV 2016)*. Volume 9908 of Springer LNCS. (2016) 354–370
28. Yu, F., Koltun, V.: Multi-scale context aggregation by dilated convolutions. *arXiv preprint arXiv:1511.07122* (2015)
29. Yu, F., Koltun, V., Funkhouser, T.: Dilated residual networks. In: *Proc. Computer Vision and Pattern Recognition (CVPR 2017)*. (2017) 472–480
30. Mehta, S., Rastegari, M., Caspi, A., Shapiro, L., Hajishirzi, H.: ESPNet: Efficient spatial pyramid of dilated convolutions for semantic segmentation. In: *Proc. European Conference on Computer Vision (ECCV 2018)*. (2018) 552–568
31. Zhang, R., Tang, S., Zhang, Y., Li, J., Yan, S.: Scale-adaptive convolutions for scene parsing. In: *Proc. International Conference on Computer Vision (ICCV 2017)*. (2017) 2031–2039
32. Wang, H., Kembhavi, A., Farhadi, A., Yuille, A.L., Rastegari, M.: ELASTIC: Improving CNNs with dynamic scaling policies. In: *Proc. Computer Vision and Pattern Recognition (CVPR 2019)*. (2019) 2258–2267
33. Chen, Y., Fang, H., Xu, B., Yan, Z., Kalantidis, Y., Rohrbach, M., Yan, S., Feng, J.: Drop an octave: Reducing spatial redundancy in convolutional neural networks with octave convolution. In: *Proc. International Conference on Computer Vision (ICCV 2019)*. (2019)
34. Bruna, J., Mallat, S.: Invariant scattering convolution networks. *IEEE Trans. Pattern Analysis and Machine Intell.* **35** (2013) 1872–1886
35. Sifre, L., Mallat, S.: Rotation, scaling and deformation invariant scattering for texture discrimination. In: *Proc. Computer Vision and Pattern Recognition (CVPR 2013)*. (2013) 1233–1240
36. Oyallon, E., Mallat, S.: Deep roto-translation scattering for object classification. In: *Proc. Computer Vision and Pattern Recognition (CVPR 2015)*. (2015) 2865–2873
37. Luan, S., Chen, C., Zhang, B., Han, J., Liu, J.: Gabor convolutional networks. *IEEE Trans. Pattern Analysis and Machine Intell.* **27** (2018) 4357–4366
38. Shelhamer, E., Wang, D., Darrell, T.: Blurring the line between structure and learning to optimize and adapt receptive fields. *arXiv preprint arXiv:1904.11487* (2019)
39. Henriques, J.F., Vedaldi, A.: Warped convolutions: Efficient invariance to spatial transformations. In: *International Conference on Machine Learning*. Volume 70. (2017) 1461–1469

40. Esteves, C., Allen-Blanchette, C., Zhou, X., Daniilidis, K.: Polar transformer networks. In: International Conference on Learning Representations (ICLR 2018). (2018)
41. Poggio, T.A., Anselmi, F.: Visual Cortex and Deep Networks: Learning Invariant Representations. MIT Press (2016)
42. Laptev, D., Savinov, N., Buhmann, J.M., Pollefeys, M.: TI-pooling: Transformation-invariant pooling for feature learning in convolutional neural networks. In: Proc. Computer Vision and Pattern Recognition (CVPR 2016). (2016) 289–297
43. Cohen, T., Welling, M.: Group equivariant convolutional networks. In: International Conference on Machine Learning (ICML 2016). (2016) 2990–2999
44. Kondor, R., Trivedi, S.: On the generalization of equivariance and convolution in neural networks to the action of compact groups. In: International Conference on Machine Learning (ICML 2018). (2018)
45. Roux, N.L., Bengio, Y.: Continuous neural networks. In: Artificial Intelligence and Statistics (AISTATS 2007). Volume 2 of Proc. of Machine Learning Research. (2007) 404–411
46. Shocher, A., Feinstein, B., Haim, N., Irani, M.: From discrete to continuous convolution layers. arXiv preprint arXiv:2006.11120 (2020)
47. Iijima, T.: Basic theory on normalization of pattern (in case of typical one-dimensional pattern). Bulletin of the Electrotechnical Laboratory **26** (1962) 368–388 (in Japanese).
48. Witkin, A.P.: Scale-space filtering. In: Proc. 8th Int. Joint Conf. Art. Intell., Karlsruhe, Germany (1983) 1019–1022
49. Koenderink, J.J.: The structure of images. Biological Cybernetics **50** (1984) 363–370
50. Babaud, J., Witkin, A.P., Baudin, M., Duda, R.O.: Uniqueness of the Gaussian kernel for scale-space filtering. IEEE Trans. Pattern Analysis and Machine Intell. **8** (1986) 26–33
51. Koenderink, J.J., van Doorn, A.J.: Generic neighborhood operators. IEEE Trans. Pattern Analysis and Machine Intell. **14** (1992) 597–605
52. Lindeberg, T.: Scale-Space Theory in Computer Vision. Springer (1993)
53. Lindeberg, T.: Scale-space theory: A basic tool for analysing structures at different scales. Journal of Applied Statistics **21** (1994) 225–270 Also available from <http://www.csc.kth.se/~tony/abstracts/Lin94-SI-abstract.html>.
54. Florack, L.M.J.: Image Structure. Series in Mathematical Imaging and Vision. Springer (1997)
55. ter Haar Romeny, B.: Front-End Vision and Multi-Scale Image Analysis. Springer (2003)
56. Lindeberg, T.: Generalized Gaussian scale-space axiomatics comprising linear scale-space, affine scale-space and spatio-temporal scale-space. Journal of Mathematical Imaging and Vision **40** (2011) 36–81
57. Lindeberg, T.: A computational theory of visual receptive fields. Biological Cybernetics **107** (2013) 589–635
58. Schiele, B., Crowley, J.: Recognition without correspondence using multidimensional receptive field histograms. International Journal of Computer Vision **36** (2000) 31–50
59. Dalal, N., Triggs, B.: Histograms of oriented gradients for human detection. In: Proc. Computer Vision and Pattern Recognition (CVPR 2005). Volume 1. (2005) 886–893

- 60. Lindeberg, T.: Normative theory of visual receptive fields. *Heliyon* (2021) Earlier manuscript in arXiv:1701.06333.
- 61. Jacobsen, J.J., van Gemert, J., Lou, Z., Smeulders, A.W.M.: Structured receptive fields in CNNs. In: *Proc. Computer Vision and Pattern Recognition (CVPR 2016)*. (2016) 2610–2619
- 62. LeCun, Y., Bottou, L., Bengio, Y., Haffner, P.: Gradient-based learning applied to document recognition. *Proceedings of the IEEE* **86** (1998) 2278–2324
- 63. Kingma, P.D., Ba, J.: Adam: A method for stochastic optimization. In: *International Conference for Learning Representations (ICLR 2015)*. (2015)
- 64. Lindeberg, T.: Scale-space for discrete signals. *IEEE Trans. Pattern Analysis and Machine Intell.* **12** (1990) 234–254
- 65. Lindeberg, T.: Discrete derivative approximations with scale-space properties: A basis for low-level feature extraction. *Journal of Mathematical Imaging and Vision* **3** (1993) 349–376
- 66. Jansson, Y., Lindeberg, T.: MNISTLargeScale dataset (2020) Available at: <https://www.zenodo.org/record/3820247>.
- 67. Lindeberg, T.: Scale selection. In Ikeuchi, K., ed.: *Computer Vision*. Springer (2021) doi:10.1007/978-3-030-03243-2\_242-1.
- 68. Loog, M., Li, Y., Tax, D.: Maximum membership scale selection. In: *Multiple Classifier Systems*. Volume 5519 of Springer LNCS. (2009) 468–477
- 69. Li, Y., Tax, D.M.J., Loog, M.: Scale selection for supervised image segmentation. *Image and Vision Computing* **30** (2012) 991–1003